
GI-NAS: Boosting Gradient Inversion Attacks through Adaptive Neural Architecture Search

Wenbo Yu^{1¶}, Hao Fang^{2¶}, Bin Chen^{1§}, Xiaohang Sui¹, Chuan Chen³,
Hao Wu², Shu-Tao Xia², Ke Xu⁴

¹School of Computer Science and Technology, Harbin Institute of Technology, Shenzhen

²Tsinghua Shenzhen International Graduate School, Tsinghua University

³School of Computer Science and Engineering, Sun Yat-Sen University

⁴Department of Computer Science and Technology, Tsinghua University

{yuwenbo, suixiaohang}@stu.hit.edu.cn; {fang-h23, wu-h22}@mails.tsinghua.edu.cn;
chenbin2021@hit.edu.cn; chenchuan@mail.sysu.edu.cn; xiaast@sz.tsinghua.edu.cn;
xuke@tsinghua.edu.cn

Abstract

Gradient Inversion Attacks invert the transmitted gradients in Federated Learning (FL) systems to reconstruct the sensitive data of local clients and have raised considerable privacy concerns. A majority of gradient inversion methods rely heavily on explicit prior knowledge (e.g., a well pre-trained generative model), which is often unavailable in realistic scenarios. To alleviate this issue, researchers have proposed to leverage the implicit prior knowledge of an over-parameterized network. However, they only utilize a fixed neural architecture for all the attack settings. This would hinder the adaptive use of implicit architectural priors and consequently limit the generalizability. In this paper, we further exploit such implicit prior knowledge by proposing Gradient Inversion via Neural Architecture Search (GI-NAS), which adaptively searches the network and captures the implicit priors behind neural architectures. Extensive experiments verify that our proposed GI-NAS can achieve superior attack performance compared to state-of-the-art gradient inversion methods, even under more practical settings with high-resolution images, large-sized batches, and advanced defense strategies.

1 Introduction

Federated Learning (FL) [1, 2, 3] serves as an efficient collaborative learning framework where multiple participants cooperatively train a global model and only the computed gradients are exchanged. By adopting this distributed paradigm, FL systems fully leverage the huge amounts of data partitioned across various clients for enhanced model efficacy and tackle the separateness of data silos [4]. Moreover, since merely the gradients instead of the intimate data are uploaded to the server, the user privacy seems to be safely guaranteed as the private data is only available at the client side.

However, FL systems are actually not so reliable as expected. Extensive studies have discovered that even the conveyed gradients can disclose the sensitive information of users. Early works [5, 6, 7, 8] involve inferring the existence of certain samples in the dataset (i.e., Membership Inference Attacks [9]) or further revealing some properties of the private training set (i.e., Property Inference Attacks [10]) from the uploaded gradients. But unlike the above inference attacks that only partially reveal

[¶]The first two authors contributed equally to this work. Wenbo Yu performed this work while pre-admitted to Tsinghua Shenzhen International Graduate School.

[§]Corresponding author.

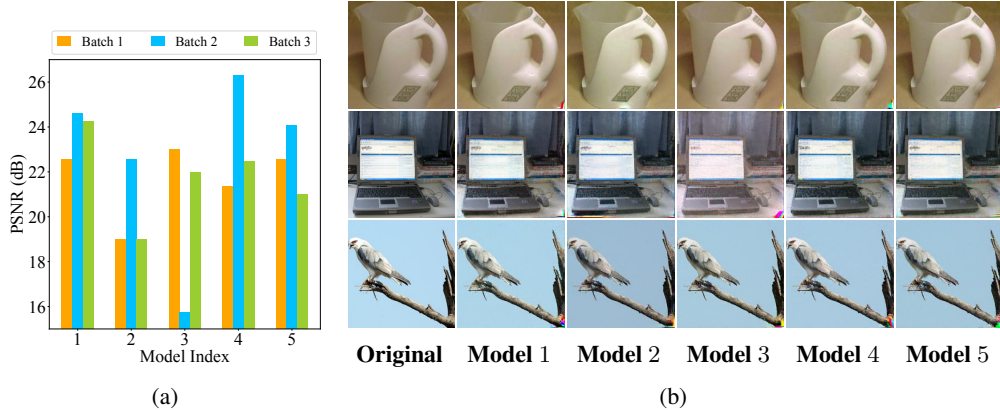


Figure 1: Results when attacking 3 different batches by 5 different models on ImageNet. (a) shows the quantitative comparison. (b) presents the qualitative comparison, where the images of the first row, the second row, and the third row are respectively from Batch 1, Batch 2, and Batch 3.

limited information of the private data, Gradient Inversion Attacks stand out as a more threatening privacy risk as they can completely reconstruct the sensitive data by inverting the gradients.

Zhu *et al.* [11] first formulate gradient inversion as an optimization problem and recover the intimate training images by minimizing the gradient matching loss (i.e., the distance between the dummy gradients and the real gradients) with image pixels regarded as trainable parameters. Ensuing works improve the attack performance on the basis of Zhu *et al.* [11] by designing label extraction techniques [12], switching the distance metric and introducing regularization [13], or considering larger batch sizes settings [14], but still restrict their optimizations in the pixel space. To fill this gap, recent studies [15, 16, 17] propose to explore various search algorithms within the Generative Adversarial Networks (GAN) [18, 19] to leverage the rich prior knowledge encoded in the pre-trained generative models. While incorporating these explicit priors indeed improves the attack performance, it is usually tough to pre-prepare such prerequisites in realistic FL scenarios where the data distribution at the client side is likely to be complex or unknown to the attackers. Therefore, Zhang *et al.* [20] propose to employ an over-parameterized convolutional network for gradient inversion and directly optimize the excessive network parameters on a fixed input, which does not require any explicit prior information but still outperforms GAN-based attacks. The reason behind this is that the structure of a convolutional network naturally captures image statics prior to any learning [21] and Zhang *et al.* [20] leverage this characteristic as implicit prior knowledge. However, Zhang *et al.* [20] only utilize a fixed network for all the attack settings, regardless of the specific batch to recover. An intuitive question naturally arises: *can we adaptively search the architecture of the over-parameterized network to better capture the implicit prior knowledge for each reconstructed batch?*

In Figure 1, we randomly select 5 over-parameterized networks with different architectures to attack 3 different batches. All the networks are optimized for the same number of iterations on ImageNet [22]. The results indicate that the PSNR performance varies significantly when changing the architectures. For the same batch, various architectures can hold remarkably different implicit priors on it. Besides, since the optimal models for Batch 1, Batch 2, and Batch 3 are respectively Model 3, Model 4, and Model 1, there exists no network that can consistently perform the best on all the given batches. Thus, the changeless adoption of architecture by Zhang *et al.* [20] lacks optimality under dynamic scenarios and it is of great significance to adaptively select the most suitable architecture for each batch.

Inspired by the above phenomenons, we propose a novel gradient inversion method, named **Gradient Inversion via Neural Architecture Search (GI-NAS)**, to better match each batch with the optimal model architecture. Specifically, we first enlarge the potential search space for the over-parameterized network by designing different upsampling modules and skip connection patterns. To reduce the computational overhead, we utilize a training-free search strategy that compares the initial gradient matching loss for a given batch over all the candidates and selects the best of them for the final optimization. We further provide experimental evidence that such a metric highly correlates with the real performance. We also consider more rigorous and realistic scenarios where the victims may hold high-resolution images and large-sized batches for training, and evaluate advanced defense strategies.

Extensive experiments validate that GI-NAS can achieve state-of-the-art performance compared to existing gradient inversion methods. Our main contributions can be summarized as follows:

- We systematically analyze existing methods, emphasize the necessity of equipping image batch recovery with the optimal model structure, and propose GI-NAS to boost gradient inversion through neural architectural search.
- We expand the model search space by considering different upsampling units and skip connection modes, and utilize a training-free search that regards the initial gradient matching loss as the search metric. We also provide experimental evidence that such a metric highly correlates with the real performance.
- Numerous experimental results demonstrate that GI-NAS outperforms state-of-the-art gradient inversion methods, even under extreme settings with high-resolution images, large-sized batches, and advanced defense strategies. The ablation study further demonstrates the significance of our optimal architecture search.

2 Related Work

Gradient Inversion Attacks and Defenses. Zhu *et al.* [11] first propose to restore the private samples via iterative optimization for pixel-level reconstruction, yet limited to low-resolution and single images. Geiping *et al.* [13] empirically decompose the gradient vector by its norm magnitude and updating direction, and succeed on high-resolution ImageNet [22] through the angle-based loss design. Furthermore, Yin *et al.* [14] extend the attacks to the batch-level inversion through the group consistency regularization and the improved batch label inference algorithm [12]. With strong handcrafted explicit priors (e.g., fidelity regularization, BN statistics), they accurately realize batch-level reconstruction with detailed semantic features allocated to all the individual images in a batch. Subsequent studies [15, 16, 17] leverage pre-trained GAN models as generative priors [23, 24, 25] to enhance the attacks. Besides, Hatamizadeh *et al.* [26] apply gradient inversion to ViT [27] and uncover its vulnerability through component-wise analysis. Current defenses focus on gradient perturbation to alleviate the impact of gradient inversion with degraded gradients [28, 29, 30]. Gaussian Noise [31] and Gradient Clipping [32] are common techniques in Differential Privacy (DP) that effectively constrain the attackers from learning through the released gradients. Gradient Sparsification [33, 34] prunes the gradients through a given threshold, and Soteria [35] edits the gradients from the aspect of learned representations. These defenses significantly reduce the information carried in the gradients and can be a great challenge to gradient inversion attacks.

Neural Architecture Search (NAS). By automatically searching the optimal model architecture, NAS algorithms prove to be significantly effective in multiple visual tasks such as image restoration [36, 37], semantic segmentation [38, 39, 40], and image classification [41, 42, 43, 44]. In image classification tasks, Zoph *et al.* [42, 44] regularize the search space to a convolutional cell and construct a better architecture stacked by these cells using an RNN controller. For semantic segmentation tasks, Liu *et al.* [39] search for the optimal network on the level of hierarchical network architecture and extend NAS to dense image prediction. In terms of image restoration tasks, the HiNAS proposed by Zhang *et al.* [45] firstly employs the gradient-based NAS on the denoising task. Suganuma *et al.* [36] exploit a better Convolutional Autoencoders (CAE) with standard network components through the evolutionary search, while Chu *et al.* [37] discover a competitive lightweight model for image super-resolution via both micro and macro architecture search.

Existing NAS algorithms adopt different search strategies to exploit the architecture search space, including evolutionary methods [46, 47, 48, 49, 50, 51, 52], Bayesian optimization [53, 54, 55], Reinforcement Learning (RL) [56, 57, 58, 42, 44], and gradient-based search [59, 60, 61, 62, 63]. Different RL-based methods vary in the way to represent the agent’s policy and the optimization process. Zoph *et al.* [42] utilize the RNN network to sequentially encode the neural architecture and train the network with the REINFORCE policy gradient algorithm [64]. Baker *et al.* [56] adopt Q-learning [65, 66] to train the policy network and realize competitive model design. Current evolutionary approaches [48, 36] explore neural structures through mutations on layers and hyper-parameters and differ in their evolution strategies. Notably, recent works [67, 68, 69] propose training-free NAS methods to mitigate the issue of huge computational expense. Instead of training from scratch, they evaluate the searched networks by some empirically designed metrics that can reflect model effectiveness. In this paper, we adopt the initial gradient matching loss as the training-

free metric for our network search and provide experimental evidence in the later section that such a search metric highly correlates with the actual performance.

3 Problem Formulation

Basics of Gradient Inversion. We consider the training process of a classification model f_θ parameterized by θ in FL scenarios. The real gradients \mathbf{g} are calculated from a private batch (with real images \mathbf{x} and real labels \mathbf{y}) at the client side. The universal goal of gradient inversion attacks is to search for some fake images $\hat{\mathbf{x}} \in \mathbb{R}^{B \times H \times W \times C}$ with labels $\hat{\mathbf{y}} \in \{0, 1\}^{B \times L}$ so that $(\hat{\mathbf{x}}, \hat{\mathbf{y}})$ can be close to (\mathbf{x}, \mathbf{y}) as much as possible, where B, H, W, C , and L are respectively batch size, image height, image width, number of channels, and number of classes. This can be realized by minimizing the gradient matching loss [11]:

$$\hat{\mathbf{x}}^*, \hat{\mathbf{y}}^* = \arg \min_{\hat{\mathbf{x}}, \hat{\mathbf{y}}} \mathcal{D}(\nabla_\theta \mathcal{L}(f_\theta(\hat{\mathbf{x}}), \hat{\mathbf{y}}), \mathbf{g}), \quad (1)$$

where $\mathcal{D}(\cdot, \cdot)$ is the distance metric (e.g., l_2 -norm loss, cosine-similarity loss) for the gradient matching loss and $\mathcal{L}(\cdot, \cdot)$ is the loss function of the global model f_θ .

Previous works [12, 14] in this field have revealed that the ground truth labels \mathbf{y} can be directly inferred from the uploaded gradients \mathbf{g} . Therefore, the formulation in (1) can be simplified as:

$$\hat{\mathbf{x}}^* = \arg \min_{\hat{\mathbf{x}}} \mathcal{D}(F(\hat{\mathbf{x}}), \mathbf{g}), \quad (2)$$

where $F(\hat{\mathbf{x}}) = \nabla_\theta \mathcal{L}(f_\theta(\hat{\mathbf{x}}), \hat{\mathbf{y}})$ calculates the gradients of f_θ provided with $\hat{\mathbf{x}}$.

The key challenge of (2) is that gradients only provide limited information of private data and there can even exist a pair of different data having the same gradients [70]. To mitigate this issue, subsequent works incorporate various regularization terms (e.g., total variation loss [13], group consistency loss [14]) as prior knowledge. Therefore, the overall optimization becomes:

$$\hat{\mathbf{x}}^* = \arg \min_{\hat{\mathbf{x}}} \mathcal{D}(F(\hat{\mathbf{x}}), \mathbf{g}) + \lambda \mathcal{R}_{prior}(\hat{\mathbf{x}}), \quad (3)$$

where $\mathcal{R}_{prior}(\cdot)$ is the introduced regularization that can establish some image priors for the attacks, and λ is the weight factor.

GAN-based Gradient Inversion. Nevertheless, the optimization of (3) is still limited in the pixel space. Given a well pre-pretrained GAN, an instinctive idea is to swift the optimization from the pixel space to the GAN latent space:

$$\mathbf{z}^* = \arg \min_{\mathbf{z}} \mathcal{D}(F(G_\omega(\mathbf{z})), \mathbf{g}) + \lambda \mathcal{R}_{prior}(G_\omega(\mathbf{z})), \quad (4)$$

where G_ω and $\mathbf{z} \in \mathbb{R}^{B \times l}$ are respectively the generator and the latent vector of the pre-trained GAN. By reducing the optimization space from $\mathbb{R}^{B \times H \times W \times C}$ to $\mathbb{R}^{B \times l}$, (4) overcomes the uncertainty of directly optimizing the extensive pixels and exploits the abundant prior knowledge encoded in the pre-trained GAN. Based on this, recently emerged GAN-based attacks [15, 16] explore various search strategies within the pre-trained GAN to utilize its expression ability.

Gradient Inversion via Over-parameterized Networks. But as previously mentioned, incorporating such GAN priors is often impractical in realistic scenarios where the distribution of \mathbf{x} is likely to be mismatched with the training data of the pre-trained GAN. Furthermore, it has already been discovered in [20] that explicitly introducing regularization in (3) or (4) may not necessarily result in convergence towards \mathbf{x} , as even ground truth images can not guarantee minimal loss when $\mathcal{R}_{prior}(\cdot)$ is added. To mitigate these issues, Zhang *et al.* [20] propose to leverage an over-parameterized network as implicit prior knowledge:

$$\phi^* = \arg \min_{\phi} \mathcal{D}(F(G_{over}(\mathbf{z}_0; \phi)), \mathbf{g}), \quad (5)$$

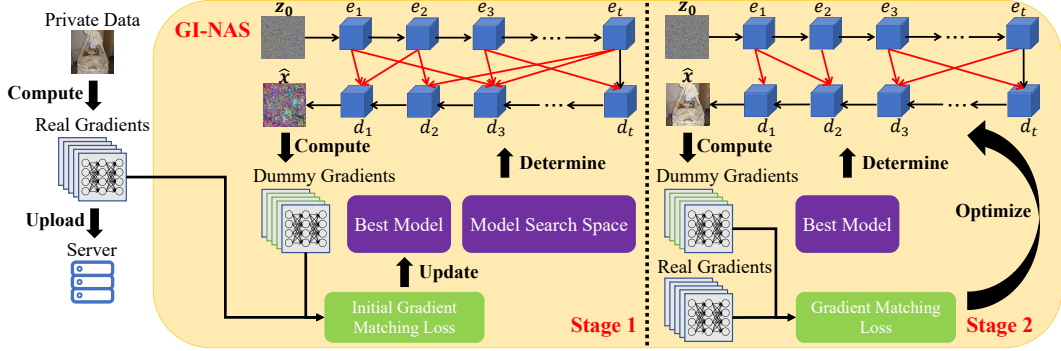


Figure 2: Overview of the proposed GI-NAS attack. We leverage a two-stage strategy for private batch recovery. In the first stage, we traverse the model search space and calculate the initial gradient matching loss (i.e., our training-free metric) of each model based on the fixed input \mathbf{z}_0 . We regard the model that achieves the minimal initial loss as our best model, for its performance at the start can stand from numerous candidates. In the second stage, we adopt the architecture of the previously found best model and optimize its excessive parameters to reconstruct the private data.

where G_{over} is the over-parameterized convolutional network with excessive parameters ϕ , and \mathbf{z}_0 is the randomly generated but fixed latent code. Note that the regularization term is omitted in (5). This is because the architecture of G_{over} itself can serve as implicit regularization, for convolutional networks have been proven to possess implicit priors that prioritize clean images rather than noise as shown in [21]. Thus, the generated images that highly resemble the ground truth images can be obtained through $\hat{\mathbf{x}}^* = G_{over}(\mathbf{z}_0; \phi^*)$. However, only a changeless over-parameterized network is employed for all the attack settings in [20]. As previously shown in Figure 1, although the network is over-parameterized, the attack performance exhibits significant differences when adopting different architectures. Therefore, we propose to further exploit such implicit priors by searching the optimal over-parameterized network G_{opt} for each batch. We will discuss how to realize this in Section 4.

4 Method

Our proposed GI-NAS attack is carried out in two stages. In the first stage, we conduct our architecture search to decide the optimal model G_{opt} . Given that the attackers may only hold limited resources, we utilize the initial gradient matching loss as the training-free search metric to reduce the computational overhead. In the second stage, we iteratively optimize the parameters of the selected model G_{opt} to recover the sensitive data. Figure 2 illustrates the overview of our method.

4.1 Training-free Optimal Model Search

4.1.1 Model Search Space Design

One crucial factor for NAS is that the potential search space is large and diverse enough to cover the optimal design. Therefore, we adopt U-Net [71], a typical convolutional neural architecture as the fundamental of our model search, since the skip connection patterns between its encoders and decoders can provide adequate alternatives of model structure. Besides, the configurations of the upsampling modules (e.g., kernel size, activation function) can also enable numerous possibilities when combined. Following previous methods [72, 73], we enlarge the search space of our model from two aspects, namely *Upsampling Modules* and *Skip Connection Patterns*.

Search Space for Upsampling Modules. We decompose the upsampling operations into five key components: feature upsampling, feature transformation, activation function, kernel size, and dilation rate. Then, we allocate a series of possible options to each of these components. When deciding on feature upsampling, we choose from commonly used interpolation techniques, such as bilinear interpolation, bicubic interpolation, and nearest-neighbour interpolation. As for feature transformation, we choose from classical convolution techniques, such as 2D convolution, separable convolution, and depth-wise convolution. As regards activation function, we select from ReLU, LeakyReLU, PReLU, etc. Furthermore, we supply kernel size and dilation rate with more choices,

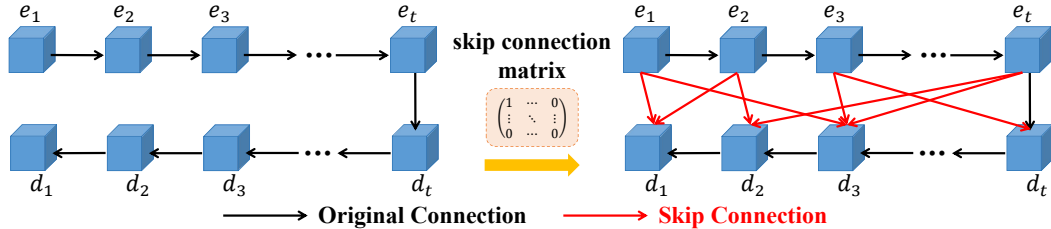


Figure 3: The design of search space for skip connection patterns. Different skip connection patterns are determined by the skip connection matrix $\mathbf{A} \in \{0, 1\}^{t \times t}$. $\mathbf{A}_{ij} = 1$ indicates that there exists a skip connection from e_i to d_j and $\mathbf{A}_{ij} = 0$ means that there isn't such a skip connection.

such as 1×1 , 3×3 , or 5×5 for kernel size and 1, 3, or 5 for dilation rate. The combination of these flexible components can contribute to the diversity of upsampling modules.

Search Space for Skip Connection Patterns. We assume that there are t levels of encoders and decoders in total, and denote them as e_1, e_2, \dots, e_t and d_1, d_2, \dots, d_t . As shown in Figure 3, We consider different skip connection patterns between encoders and decoders. To represent each of these patterns, we define a skip connection matrix $\mathbf{A} \in \{0, 1\}^{t \times t}$ that serves as a mask to determine whether there will be new residual connections [74] between pairs of encoders and decoders. More concretely, $\mathbf{A}_{ij} = 1$ indicates that there exists a skip connection from e_i to d_j and $\mathbf{A}_{ij} = 0$ means that there isn't such a skip connection. As the shapes of feature maps across different network levels can vary significantly (e.g., 64×64 for the output of e_i and 256×256 for the input of d_j), we introduce connection scale factors to tackle this inconsistency and decompose all the possible scale factors into a series of $2 \times$ upsampling operations or downsampling operations with shared weights. By allocating 0 or 1 to each of the t^2 bits in \mathbf{A} , we broaden the search space of skip connection patterns as there are 2^{t^2} possibilities altogether and we only need to sample a portion of them.

4.1.2 Optimal Model Selection

We build up our model search space \mathcal{M} by combining the possibilities of the aforementioned upsampling modules and skip connection patterns. We assume that the size of our model search space is n and the candidates inside it are denoted as $\mathcal{M} = \{G_1, G_2, \dots, G_n\}$. We first sample the latent code \mathbf{z}_0 from the Gaussian distribution and freeze its values on all the models for fair comparison. We then traverse the model search space and calculate the initial gradient matching loss of each individual G_r ($1 \leq r \leq n$):

$$\mathcal{L}_{grad}(G_r) = \mathcal{D}(\mathcal{T}(F(G_r(\mathbf{z}_0; \phi_r))), \mathbf{g}), \quad (6)$$

where $\mathcal{L}_{grad}(\cdot)$ is the gradient matching loss, $\mathcal{T}(\cdot)$ is the estimated gradient transformation [15], and ϕ_r are the parameters of G_r . Here we introduce $\mathcal{T}(\cdot)$ to estimate the gradient transformation following the previous defense auditing work [15], since the victims may apply defense strategies to \mathbf{g} (e.g., Gradient Clipping [31]) and only release disrupted forms of gradients. Empirically, the model that can perform the best at the start and stand out from numerous candidates is likely to have better implicit architectural priors with respect to the private batch. Therefore, we regard the model that achieves the minimal initial loss as our best model G_{opt} and update our selection during the traversal. Since only the initial loss is calculated and no back-propagation is involved, this search process is training-free and hence computationally efficient.

4.2 Private Batch Recovery via the Optimal Model

After deciding on the optimal model G_{opt} , we iteratively optimize its parameters to minimize the gradient matching loss:

$$\gamma_{k+1} = \gamma_k - \eta \nabla_{\gamma_k} \mathcal{L}_{grad}(G_{opt}), \quad (7)$$

Table 1: Quantitative comparison of GI-NAS to state-of-the-art gradient inversion methods on CIFAR-10 (32×32) and ImageNet (256×256) with the default batch size $B = 4$.

Metric	CIFAR-10						ImageNet					
	IG	GI	GGL	GIAS	GION	GI-NAS	IG	GI	GGL	GIAS	GION	GI-NAS
PSNR \uparrow	16.3188	15.4613	12.4938	17.3687	30.8652	35.9883	7.9419	8.5070	11.6255	10.0602	21.9942	23.2578
SSIM \uparrow	0.5710	0.5127	0.3256	0.6239	0.9918	0.9983	0.0815	0.1157	0.2586	0.2408	0.6188	0.6848
FSIM \uparrow	0.7564	0.7311	0.6029	0.7800	0.9960	0.9991	0.5269	0.5299	0.5924	0.5719	0.8198	0.8513
LPIPS \downarrow	0.4410	0.4878	0.5992	0.4056	0.0035	0.0009	0.7194	0.7168	0.6152	0.6563	0.4605	0.3952

where γ are the parameters of G_{opt} , η is the learning rate, and k is the number of iterations. Once the above process converges and we obtain γ^* that satisfy the minimum loss, the private batch can be reconstructed by $\hat{\mathbf{x}}^* = G_{opt}(\mathbf{z}_0; \gamma^*)$.

5 Experiments

5.1 Setup

Experimental Details. We evaluate our method on CIFAR-10 [75] and ImageNet [22] with the resolution of 32×32 and 256×256 . Unlike many previous methods [16, 17] that scale down the ImageNet images to 64×64 , here we emphasize that we adopt the high-resolution version of ImageNet. Thus, our setting is more rigorous and realistic. Following previous gradient inversion works [11, 20], we adopt ResNet-18 [74] as our global model and utilize the same preprocessing procedures. We set the search space size as $n = 5000$ and randomly generate the alternative models by arbitrarily changing the options of upsampling modules and skip connection patterns.

State-of-the-art Baselines for Comparison. We implement the following gradient inversion methods: (1) *IG (Inverting Gradients)* [13]: pixel-level reconstruction with angle-based loss function; (2) *GI (GradInversion)* [14]: realizing batch-level restoration via multiple regularization priors; (3) *GGL (Generative Gradient Leakage)* [15]: employing strong GAN priors to produce high-fidelity images under severe defense strategies; (4) *GIAS (Gradient Inversion in Alternative Space)* [16]: searching the optimal latent code while optimizing in the generator parameter space; (5) *GION (Gradient Inversion via Over-parameterized Networks)* [20]: designing an over-parameterized convolutional network with excessive parameters and employing a fixed network architecture as implicit regularization. Note that when implementing GAN-based methods such as GGL and GIAS, we adopt BigGAN [76] pre-trained on ImageNet, which may result in mismatched priors when the target data is from CIFAR-10. However, such mismatch can be very common in realistic FL scenarios.

Evaluation Metrics. We utilize four metrics to measure the reconstruction results: (1) *PSNR \uparrow (Peak Signal-to-Noise Ratio)*; (2) *SSIM \uparrow (Structural Similarity Index Measure)*; (3) *FSIM \uparrow (Feature Similarity Index Measure)*; (4) *LPIPS \downarrow (Learned Perceptual Image Patch Similarity)* [77]. Note that " \downarrow " indicates that the lower the metric, the better the attack performance while " \uparrow " indicates that the higher the metric, the better the attack performance.

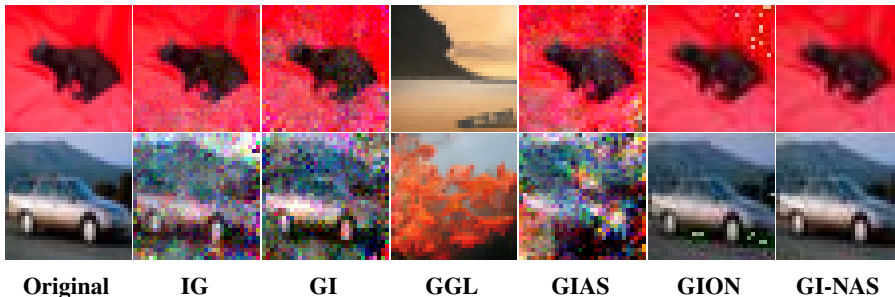


Figure 4: Qualitative comparison of GI-NAS to state-of-the-art gradient inversion methods on CIFAR-10 (32×32) with the default batch size $B = 4$.

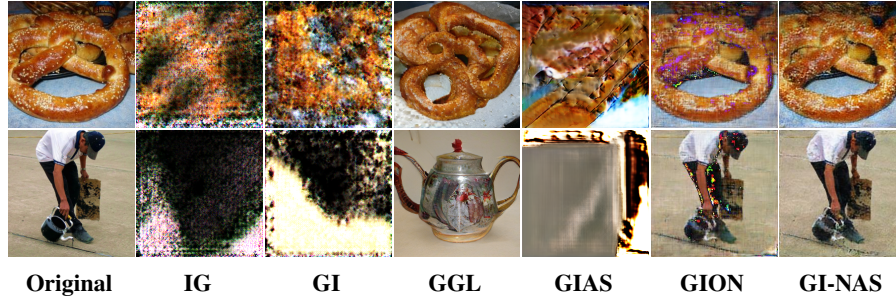


Figure 5: Qualitative comparison of GI-NAS to state-of-the-art gradient inversion methods on ImageNet (256×256) with the default batch size $B = 4$.

5.2 Comparison with State-of-the-art Methods

Firstly, we compare GI-NAS with state-of-the-art gradient inversion methods on CIFAR-10. From Table 1, we conclude that GI-NAS achieves the best results with significant performance improvement. For instance, we realize a 5.12 dB PSNR increase than GION, and our LPIPS value is 74.3% smaller than that of GION. These prove that in contrast to GION that optimizes on a fixed network, our NAS strategy indeed comes into effect and better leverages the implicit architectural priors.

We also discover that the GAN-based method GGL underperforms the previous GAN-free methods (i.e., IG and GI). This is because GGL utilizes BigGAN [76] pre-trained on ImageNet for generative priors in our settings, which has an inherent distribution bias with the target CIFAR-10 data domain. Besides, GGL only optimizes the latent vectors and cannot dynamically handle the mismatch between the training data of GAN and the target data. In contrast, GIAS optimizes both the latent vectors and the GAN parameters, which can reduce the distribution divergence and alleviate such mismatch to some extent. Therefore, although also GAN-based, GIAS exhibits much better performance than GGL on CIFAR-10. Figure 4 shows the qualitative comparison of different methods on CIFAR-10. We notice that GI-NAS outperforms all the compared methods in terms of pixel-level recovery. Although GION also achieves results relatively close to the ground truth images, it still suffers from a few flaws and artifacts in some areas compared to GI-NAS. This again verifies the necessity of searching the optimal architecture. We also note that there are huge differences between the images generated by GGL and the original images due to the mismatched GAN priors that we have previously discussed.

High-Resolution Images Recovery. We then consider a more challenging situation and compare various methods on ImageNet with the resolution of 256×256 . As shown in Table 1, most methods encounter significant performance decline when attacking high-resolution images. The amplification of image pixels greatly increases the complexity of reconstruction tasks and thus obstructs the optimization process for optimal images. But GI-NAS still achieves the best attack results, with a PSNR increase of 1.26 dB than GION. From Figure 5, we notice that GI-NAS can recover the rich semantic features in the original images, with fewer speckles or smudges than GION. This is because GI-NAS has discovered the architecture that better suits each batch and thus handles the details better.

Extension to Larger Batch Sizes. As shown in Table 2, we extend GI-NAS to larger batch sizes on ImageNet, which is more in line with the actual training process of FL systems. We observe that the performance of most methods degrades as the batch size increases, while GI-NAS is insusceptible

Table 2: Quantitative comparison of GI-NAS to state-of-the-art gradient inversion methods on ImageNet (256×256) with larger batch sizes when $B > 4$.

Metric	Batch Size	IG	GI	GGL	GIAS	GION	GI-NAS	Batch Size	IG	GI	GGL	GIAS	GION	GI-NAS
PSNR \uparrow	8	7.6011	8.3419	11.5454	9.6216	20.4841	20.8451	24	7.1352	7.9079	10.9910	9.6601	20.6845	21.7933
SSIM \uparrow		0.0762	0.1113	0.2571	0.2218	0.5681	0.6076		0.0549	0.0892	0.2583	0.2270	0.5868	0.6236
FSIM \uparrow		0.5103	0.5365	0.5942	0.5765	0.7908	0.8105		0.4794	0.4943	0.5811	0.5618	0.7978	0.8163
LPIPS \downarrow		0.7374	0.7251	0.6152	0.6621	0.5162	0.4613		0.7540	0.7475	0.6261	0.6667	0.5219	0.4651
PSNR \uparrow	16	7.7991	8.0233	11.4766	9.2563	20.3078	21.4267	32	7.1085	7.8752	10.8987	10.0563	16.1275	20.0011
SSIM \uparrow		0.0704	0.0952	0.2561	0.2189	0.5507	0.6141		0.0554	0.0763	0.2558	0.2361	0.3415	0.5485
FSIM \uparrow		0.5077	0.5165	0.5872	0.5832	0.7840	0.8157		0.4940	0.4951	0.5889	0.5762	0.6823	0.7819
LPIPS \downarrow		0.7424	0.7362	0.6165	0.6656	0.5313	0.4613		0.7493	0.7427	0.6296	0.6674	0.6291	0.5265

Table 3: Quantitative comparison of GI-NAS to state-of-the-art gradient inversion methods on ImageNet (256×256) under various defense strategies with the default batch size $B = 4$.

Metric	Defense	IG	GI	GGL	GIAS	GION	GI-NAS	Defense	IG	GI	GGL	GIAS	GION	GI-NAS
PSNR \uparrow		7.7020	7.4553	9.7381	6.8520	9.2449	11.2567		8.6540	8.6519	9.8019	9.7894	13.7358	15.4331
SSIM \uparrow	Gaussian	0.0311	0.0197	0.2319	0.1045	0.0277	0.0416	Gradient	0.0669	0.0627	0.2315	0.2515	0.2387	0.3154
FSIM \uparrow	Noise	0.4518	0.3804	0.5659	0.4562	0.5714	0.5846	Sparsification	0.5073	0.4696	0.5624	0.5664	0.6365	0.6786
LPIPS \downarrow		0.7775	0.8220	0.6639	0.7282	0.8033	0.7805		0.7480	0.7681	0.6589	0.6604	0.6909	0.6535
PSNR \uparrow		8.0690	7.2342	11.3215	9.7556	22.2016	23.2074		6.5675	6.6693	11.5690	9.7588	22.9617	23.7917
SSIM \uparrow	Gradient	0.0881	0.0659	0.2531	0.2547	0.6266	0.7023	Soteria	0.0323	0.0382	0.2623	0.2425	0.6698	0.7143
FSIM \uparrow	Clipping	0.5362	0.5434	0.5900	0.5794	0.8229	0.8635		0.4929	0.4454	0.5964	0.5697	0.8430	0.8658
LPIPS \downarrow		0.7227	0.7230	0.6117	0.6485	0.4603	0.3743		0.7506	0.7703	0.6031	0.6631	0.4253	0.3655

to batch sizes and continuously generates high-quality images even at $B = 32$. Besides, GI-NAS is able to acquire consistent performance gains on the basis of GION at all the given batch sizes. This further provides evidence for the necessity and effectiveness of our batch-level architecture search.

Attacks under Defense Strategies. Next, we evaluate how these attacks perform when defenses are applied on ImageNet. Following previous works [15, 11], we consider four strict defense strategies: (1) *Gaussian Noise* [31] with a standard deviation of 0.1; (2) *Gradient Clipping* [31] with a clipping bound of 4; (3) *Gradient Sparsification* [33] with a pruning rate of 90%; (4) *Representative Perturbation (Soteria)* [35] with a pruning rate of 80%. For fair comparison, we apply the estimated gradient transformation $\mathcal{T}(\cdot)$ described in (6) to all the attack methods. From Table 3, we discover that although the gradients have been disrupted by the imposed defense strategies, GI-NAS still realizes the best reconstruction effects in almost all the tested cases. The only exception is that GGL outperforms GI-NAS in terms of SSIM and LPIPS when the defense strategy is Gaussian Noise [31]. This is because the gaussian noise with a standard deviation of 0.1 can severely corrupt the gradients and the information carried inside the gradients is no longer enough for batch recovery. However, GGL only optimizes the latent vectors and can still generate natural images that possess some semantic features by the pre-trained GAN. Thus, GGL can still obtain not bad performance even though the generated images are quite dissimilar to the original ones.

5.3 Further Analysis

Effectiveness of the Training-free Metric. In Figure 6, we analyze how the initial gradient matching loss correlates with the real performance when attacking the same batch by different models on ImageNet. The Kendall’s τ [78] between these two indicators is -0.491, which means that they are highly relevant and a smaller initial loss is more likely to result in better PSNR performance.

Ablation Study. In Table 4, We report the PSNR results of GION and different variants of GI-NAS. GI-NAS* optimizes on a fixed over-parameterized network, which means that it is essentially the same as GION. GI-NAS[†] only searches the skip connection patterns while GI-NAS[‡] only searches the upsampling modules. We observe that the performance of GI-NAS* is very close to that of GION, as both of them adopt a changeless architecture. GI-NAS[†] and GI-NAS[‡] indeed improve the attacks on the basis of GION or GI-NAS*, which validates the contributions of individual search types. GI-NAS combines the above two search types and thus performs the best among all the variants.

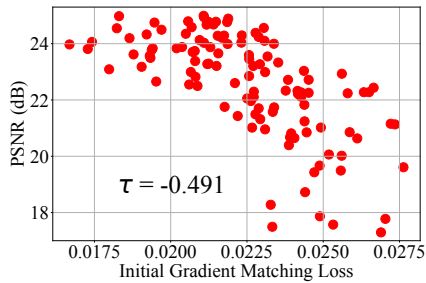


Figure 6: Correlation between the search metric and the actual performance.

Table 4: Ablation Study. We report the PSNR results of GION and different variants of GI-NAS on CIFAR-10 (32×32) and ImageNet (256×256) with the default batch size $B = 4$.

Method	Upsampling Search	Connection Search	CIFAR-10	ImageNet
GION	\times	\times	30.8652	21.9942
GI-NAS*	\times	\times	30.6514	22.0126
GI-NAS [†]	\times	\checkmark	35.4336	22.4597
GI-NAS [‡]	\checkmark	\times	35.3542	22.3992
GI-NAS	\checkmark	\checkmark	35.9883	23.2578

6 Conclusion

In this paper, we propose GI-NAS, a novel gradient inversion method that makes deeper use of the implicit architectural priors for gradient inversion. We first systematically analyze existing gradient inversion methods and emphasize the necessity of adaptive architecture search. We then build up our model search space by designing different upsampling modules and skip connection patterns. To reduce the computational overhead, we leverage the initial gradient matching loss as the training-free search metric to select the optimal model architecture and provide experimental evidence that such a metric highly correlates with the real performance. Extensive experiments prove that GI-NAS can achieve state-of-the-art performance compared to existing methods, even under more practical FL scenarios with high-resolution images, large-sized batches, and advanced defense strategies. The ablation study further demonstrates the significance of our optimal architecture search.

References

- [1] McMahan, Brendan and Moore, Eider and Ramage, Daniel and Hampson, Seth and y Arcas, Blaise Aguera. Communication-efficient learning of deep networks from decentralized data. *Artificial intelligence and statistics*, pages 1273–1282, 2017.
- [2] Zhang, Chen and Xie, Yu and Bai, Hang and Yu, Bin and Li, Weihong and Gao, Yuan. A survey on federated learning. *Knowledge-Based Systems*, pages 106775, 2021.
- [3] Li, Li and Fan, Yuxi and Tse, Mike and Lin, Kuo-Yi. A review of applications in federated learning. *Computers & Industrial Engineering*, pages 106854, 2020.
- [4] Li, Junyang and Zhang, Chaobo and Zhao, Yang and Qiu, Weikang and Chen, Qi and Zhang, Xuejun. Federated learning-based short-term building energy consumption prediction method for solving the data silos problem. *Building Simulation*, pages 1145–1159, 2022.
- [5] Melis, Luca and Song, Congzheng and De Cristofaro, Emiliano and Shmatikov, Vitaly. Exploiting Unintended Feature Leakage in Collaborative Learning. *2019 IEEE Symposium on Security and Privacy (SP)*, pages 691–706, 2019.
- [6] Nasr, Milad and Shokri, Reza and Houmansadr, Amir. Comprehensive privacy analysis of deep learning: Passive and active white-box inference attacks against centralized and federated learning. *2019 IEEE Symposium on Security and Privacy (SP)*, pages 739–753, 2019.
- [7] Lyu, Lingjuan and Yu, Han and Yang, Qiang. Threats to federated learning: A survey. *arXiv preprint arXiv:2003.02133*, 2020.
- [8] Luo, Xinjian and Wu, Yuncheng and Xiao, Xiaokui and Ooi, Beng Chin. Feature inference attack on model predictions in vertical federated learning. *2021 IEEE 37th International Conference on Data Engineering (ICDE)*, pages 181–192, 2021.
- [9] Shokri, Reza and Stronati, Marco and Song, Congzheng and Shmatikov, Vitaly. Membership Inference Attacks Against Machine Learning Models. *2017 IEEE Symposium on Security and Privacy (SP)*, pages 3–18, 2017.
- [10] Ganju, Karan and Wang, Qi and Yang, Wei and Gunter, Carl A and Borisov, Nikita. Property inference attacks on fully connected neural networks using permutation invariant representations. *Proceedings of the 2018 ACM SIGSAC conference on computer and communications security*, pages 619–633, 2018.
- [11] Zhu, Ligeng and Liu, Zhijian and Han, Song. Deep Leakage from Gradients. *Advances in Neural Information Processing Systems*, 2019.
- [12] Bo Zhao and Konda Reddy Mopuri and Hakan Bilen. iDLG: Improved Deep Leakage from Gradients. *arXiv preprint arXiv:2001.02610*, 2020.
- [13] Geiping, Jonas and Bauermeister, Hartmut and Dröge, Hannah and Moeller, Michael. Inverting gradients-how easy is it to break privacy in federated learning? *Advances in Neural Information Processing Systems*, pages 16937–16947, 2020.
- [14] Yin, Hongxu and Mallya, Arun and Vahdat, Arash and Alvarez, Jose M and Kautz, Jan and Molchanov, Pavlo. See through gradients: Image batch recovery via gradinversion. *Proceedings of the IEEE/CVF Conference on Computer Vision and Pattern Recognition*, pages 16337–16346, 2021.

- [15] Li, Zhuohang and Zhang, Jiaxin and Liu, Luyang and Liu, Jian. Auditing privacy defenses in federated learning via generative gradient leakage. *Proceedings of the IEEE/CVF Conference on Computer Vision and Pattern Recognition*, pages 10132–10142, 2022.
- [16] Jeon, Jinwoo and Lee, Kangwook and Oh, Sewoong and Ok, Jungseul and others. Gradient inversion with generative image prior. *Advances in neural information processing systems*, pages 29898–29908, 2021.
- [17] Fang, Hao and Chen, Bin and Wang, Xuan and Wang, Zhi and Xia, Shu-Tao. GIFD: A Generative Gradient Inversion Method with Feature Domain Optimization. *Proceedings of the IEEE/CVF International Conference on Computer Vision*, pages 4967–4976, 2023.
- [18] Goodfellow, Ian and Pouget-Abadie, Jean and Mirza, Mehdi and Xu, Bing and Warde-Farley, David and Ozair, Sherjil and Courville, Aaron and Bengio, Yoshua. Generative adversarial networks. *Communications of the ACM*, pages 139–144, 2020.
- [19] Creswell, Antonia and White, Tom and Dumoulin, Vincent and Arulkumaran, Kai and Sengupta, Biswa and Bharath, Anil A. Generative adversarial networks: An overview. *IEEE signal processing magazine*, pages 53–65, 2018.
- [20] Zhang, Chi and Xiaoman, Zhang and Sotthiwat, Ekanut and Xu, Yanyu and Liu, Ping and Zhen, Liangli and Liu, Yong. Generative Gradient Inversion via Over-Parameterized Networks in Federated Learning. *Proceedings of the IEEE/CVF International Conference on Computer Vision*, pages 5126–5135, 2023.
- [21] Ulyanov, Dmitry and Vedaldi, Andrea and Lempitsky, Victor. Deep image prior. *Proceedings of the IEEE conference on computer vision and pattern recognition*, pages 9446–9454, 2018.
- [22] Deng, Jia and Dong, Wei and Socher, Richard and Li, Li-Jia and Li, Kai and Fei-Fei, Li. Imagenet: A large-scale hierarchical image database. *2009 IEEE conference on computer vision and pattern recognition*, pages 248–255, 2009.
- [23] Yu, Wenbo and Chen, Bin and Zhang, Qinshan and Xia, Shu-Tao. Editable-DeepSC: Cross-Modal Editable Semantic Communication Systems. *arXiv preprint arXiv:2310.10347*, 2023.
- [24] Fang, Hao and Qiu, Yixiang and Yu, Hongyao and Yu, Wenbo and Kong, Jiawei and Chong, Baoli and Chen, Bin and Wang, Xuan and Xia, Shu-Tao. Privacy Leakage on DNNs: A Survey of Model Inversion Attacks and Defenses. *arXiv preprint arXiv:2402.04013*, 2024.
- [25] Tan, Yuqi and Peng, Yuang and Fang, Hao and Chen, Bin and Xia, Shu-Tao. WaterDiff: Perceptual Image Watermarks Via Diffusion Model. *ICASSP 2024-2024 IEEE International Conference on Acoustics, Speech and Signal Processing (ICASSP)*, pages 3250–3254, 2024.
- [26] Hatamizadeh, Ali and Yin, Hongxu and Roth, Holger R. and Li, Wenqi and Kautz, Jan and Xu, Daguang and Molchanov, Pavlo. GradViT: Gradient Inversion of Vision Transformers. *Proceedings of the IEEE/CVF Conference on Computer Vision and Pattern Recognition*, pages 10021-10030, 2022.
- [27] Han, Kai and Wang, Yunhe and Chen, Hanting and Chen, Xinghao and Guo, Jianyuan and Liu, Zhenhua and Tang, Yehui and Xiao, An and Xu, Chunjing and Xu, Yixing and others. A survey on vision transformer. *IEEE transactions on pattern analysis and machine intelligence*, pages 87–110, 2022.
- [28] Huang, Yangsibo and Gupta, Samyak and Song, Zhao and Li, Kai and Arora, Sanjeev. Evaluating gradient inversion attacks and defenses in federated learning. *Advances in Neural Information Processing Systems*, pages 7232–7241, 2021.
- [29] Zhang, Rui and Guo, Song and Wang, Junxiao and Xie, Xin and Tao, Dacheng. A survey on gradient inversion: Attacks, defenses and future directions. *arXiv preprint arXiv:2206.07284*, 2022.
- [30] Dong, Tian and Zhao, Bo and Lyu, Lingjuan. Privacy for free: How does dataset condensation help privacy? *International Conference on Machine Learning*, pages 5378–5396, 2022.
- [31] Geyer, Robin C and Klein, Tassilo and Nabi, Moin. Differentially private federated learning: A client level perspective. *arXiv preprint arXiv:1712.07557*, 2017.
- [32] Wei, Wenqi and Liu, Ling and Wu, Yanzhao and Su, Gong and Iyengar, Arun. Gradient-leakage resilient federated learning. *2021 IEEE 41st International Conference on Distributed Computing Systems (ICDCS)*, pages 797–807, 2021.

- [33] Aji, Alham Fikri and Heafield, Kenneth. Sparse communication for distributed gradient descent. *Proceedings of the 2017 Conference on Empirical Methods in Natural Language Processing*, pages 440–445, 2017.
- [34] Lin, Yujun and Han, Song and Mao, Huizi and Wang, Yu and Dally, Bill. Deep Gradient Compression: Reducing the Communication Bandwidth for Distributed Training. *International Conference on Learning Representations*, 2018.
- [35] Sun, Jingwei and Li, Ang and Wang, Binghui and Yang, Huanrui and Li, Hai and Chen, Yiran. Soteria: Provable defense against privacy leakage in federated learning from representation perspective. *Proceedings of the IEEE/CVF conference on computer vision and pattern recognition*, pages 9311–9319, 2021.
- [36] Suganuma, Masanori and Ozay, Mete and Okatani, Takayuki. Exploiting the potential of standard convolutional autoencoders for image restoration by evolutionary search. *International Conference on Machine Learning*, pages 4771–4780, 2018.
- [37] Chu, Xiangxiang and Zhang, Bo and Ma, Hailong and Xu, Ruijun and Li, Qingyuan. Fast, accurate and lightweight super-resolution with neural architecture search. *2020 25th International conference on pattern recognition (ICPR)*, pages 59–64, 2021.
- [38] Nekrasov, Vladimir and Chen, Hao and Shen, Chunhua and Reid, Ian. Fast neural architecture search of compact semantic segmentation models via auxiliary cells. *Proceedings of the IEEE/CVF conference on computer vision and pattern recognition*, pages 9126–9135, 2019.
- [39] Liu, Chenxi and Chen, Liang-Chieh and Schroff, Florian and Adam, Hartwig and Hua, Wei and Yuille, Alan L and Fei-Fei, Li. Auto-deeplab: Hierarchical neural architecture search for semantic image segmentation. *Proceedings of the IEEE/CVF conference on computer vision and pattern recognition*, pages 82–92, 2019.
- [40] Chen, Liang-Chieh and Collins, Maxwell and Zhu, Yukun and Papandreou, George and Zoph, Barret and Schroff, Florian and Adam, Hartwig and Shlens, Jon. Searching for efficient multi-scale architectures for dense image prediction. *Advances in neural information processing systems*, 2018.
- [41] Real, Esteban and Aggarwal, Alok and Huang, Yanping and Le, Quoc V. Regularized evolution for image classifier architecture search. *Proceedings of the aaai conference on artificial intelligence*, pages 4780–4789, 2019.
- [42] Zoph, Barret and Le, Quoc V. Neural architecture search with reinforcement learning. *arXiv preprint arXiv:1611.01578*, 2016.
- [43] Real, Esteban and Moore, Sherry and Selle, Andrew and Saxena, Saurabh and Suematsu, Yutaka Leon and Tan, Jie and Le, Quoc V and Kurakin, Alexey. Large-Scale Evolution of Image Classifiers. *International conference on machine learning*, pages 2902–2911, 2017.
- [44] Zoph, Barret and Vasudevan, Vijay and Shlens, Jonathon and Le, Quoc V. Learning transferable architectures for scalable image recognition. *Proceedings of the IEEE conference on computer vision and pattern recognition*, pages 8697–8710, 2018.
- [45] Zhang, Haokui and Li, Ying and Chen, Hao and Shen, Chunhua. Memory-efficient hierarchical neural architecture search for image denoising. *Proceedings of the IEEE/CVF conference on computer vision and pattern recognition*, pages 3657–3666, 2020.
- [46] Angeline, Peter J and Saunders, Gregory M and Pollack, Jordan B. An evolutionary algorithm that constructs recurrent neural networks. *IEEE transactions on Neural Networks*, pages 54–65, 1994.
- [47] Liu, Hanxiao and Simonyan, Karen and Vinyals, Oriol and Fernando, Chrisantha and Kavukcuoglu, Koray. Hierarchical representations for efficient architecture search. *arXiv preprint arXiv:1711.00436*, 2017.
- [48] Miikkulainen, Risto and Liang, Jason and Meyerson, Elliot and Rawal, Aditya and Fink, Dan and Francon, Olivier and Raju, Bala and Shahrzad, Hormoz and Navruzyan, Arshak and Duffy, Nigel and others. Evolving deep neural networks. *Artificial intelligence in the age of neural networks and brain computing*, pages 269–287, 2024.
- [49] Floreano, Dario and Dürri, Peter and Mattiussi, Claudio. Neuroevolution: from architectures to learning. *Evolutionary intelligence*, pages 47–62, 2008.

- [50] Stanley, Kenneth O and Miikkulainen, Risto. Evolving neural networks through augmenting topologies. *Evolutionary computation*, pages 99–127, 2002.
- [51] Stanley, Kenneth O and D’Ambrosio, David B and Gauci, Jason. A hypercube-based encoding for evolving large-scale neural networks. *Artificial life*, pages 185–212, 2009.
- [52] Jozefowicz, Rafal and Zaremba, Wojciech and Sutskever, Ilya. An empirical exploration of recurrent network architectures. *International conference on machine learning*, pages 2342–2350, 2015.
- [53] Bergstra, James and Yamins, Daniel and Cox, David. Making a science of model search: Hyperparameter optimization in hundreds of dimensions for vision architectures. *International conference on machine learning*, pages 115–123, 2013.
- [54] Mendoza, Hector and Klein, Aaron and Feurer, Matthias and Springenberg, Jost Tobias and Hutter, Frank. Towards automatically-tuned neural networks. *Workshop on automatic machine learning*, pages 58–65, 2016.
- [55] Domhan, Tobias and Springenberg, Jost Tobias and Hutter, Frank. Speeding up automatic hyperparameter optimization of deep neural networks by extrapolation of learning curves. *Twenty-fourth international joint conference on artificial intelligence*, 2015.
- [56] Baker, Bowen and Gupta, Otkrist and Naik, Nikhil and Raskar, Ramesh. Designing neural network architectures using reinforcement learning. *International Conference on Learning Representations*, 2016.
- [57] Cai, Han and Chen, Tianyao and Zhang, Weinan and Yu, Yong and Wang, Jun. Efficient architecture search by network transformation. *Proceedings of the AAAI conference on artificial intelligence*, 2018.
- [58] Zhong, Zhao and Yan, Junjie and Wu, Wei and Shao, Jing and Liu, Cheng-Lin. Practical block-wise neural network architecture generation. *Proceedings of the IEEE conference on computer vision and pattern recognition*, pages 2423–2432, 2018.
- [59] Liu, Hanxiao and Simonyan, Karen and Yang, Yiming. Darts: Differentiable architecture search. *arXiv preprint arXiv:1806.09055*, 2018.
- [60] Shin, Richard and Packer, Charles and Song, Dawn. Differentiable neural network architecture search. *International Conference on Learning Representations Workshop*, 2018.
- [61] Xie, Sirui and Zheng, Hehui and Liu, Chunxiao and Lin, Liang. SNAS: stochastic neural architecture search. *arXiv preprint arXiv:1812.09926*, 2018.
- [62] Cai, Han and Zhu, Ligeng and Han, Song. Proxylessnas: Direct neural architecture search on target task and hardware. *arXiv preprint arXiv:1812.00332*, 2018.
- [63] Ahmed, Karim and Torresani, Lorenzo. Maskconnect: Connectivity learning by gradient descent. *Proceedings of the European Conference on Computer Vision (ECCV)*, pages 349–365, 2018.
- [64] Williams, Ronald J. Simple statistical gradient-following algorithms for connectionist reinforcement learning. *Machine learning*, pages 229–256, 1992.
- [65] Watkins, Christopher JCH and Dayan, Peter. Q-learning. *Machine learning*, pages 279–292, 1992.
- [66] Clifton, Jesse and Laber, Eric. Q-learning: Theory and applications. *Annual Review of Statistics and Its Application*, pages 279–301, 2020.
- [67] Mellor, Joe and Turner, Jack and Storkey, Amos and Crowley, Elliot J. Neural architecture search without training. *International conference on machine learning*, pages 7588–7598, 2021.
- [68] Zhang, Miao and Su, Steven and Pan, Shirui and Chang, Xiaojun and Huang, Wei and Haf-fari, Gholamreza. Differentiable architecture search without training nor labels: A pruning perspective. *arXiv preprint arXiv:2106.11542*, 2021.
- [69] Chen, Wuyang and Gong, Xinyu and Wang, Zhangyang. Neural architecture search on imagenet in four gpu hours: A theoretically inspired perspective. *arXiv preprint arXiv:2102.11535*, 2021.
- [70] Zhu, Junyi and Blaschko, Matthew B. R-gap: Recursive gradient attack on privacy. *International Conference on Learning Representations*, 2020.

- [71] Ronneberger, Olaf and Fischer, Philipp and Brox, Thomas. U-net: Convolutional networks for biomedical image segmentation. *Medical image computing and computer-assisted intervention–MICCAI 2015: 18th international conference, Munich, Germany, October 5-9, 2015, proceedings, part III 18*, pages 234–241, 2015.
- [72] Chen, Yun-Chun and Gao, Chen and Robb, Esther and Huang, Jia-Bin. Nas-dip: Learning deep image prior with neural architecture search. *Computer Vision–ECCV 2020: 16th European Conference, Glasgow, UK, August 23–28, 2020, Proceedings, Part XVIII 16*, pages 442–459, 2020.
- [73] Arican, Metin Ersin and Kara, Ozgur and Bredell, Gustav and Konukoglu, Ender. Isnas-dip: Image-specific neural architecture search for deep image prior. *Proceedings of the IEEE/CVF Conference on Computer Vision and Pattern Recognition*, pages 1960–1968, 2022.
- [74] He, Kaiming and Zhang, Xiangyu and Ren, Shaoqing and Sun, Jian. Deep residual learning for image recognition. *Proceedings of the IEEE conference on computer vision and pattern recognition*, pages 770–778, 2016.
- [75] Krizhevsky, Alex and Hinton, Geoffrey and others. Learning multiple layers of features from tiny images. 2009.
- [76] Brock, Andrew and Donahue, Jeff and Simonyan, Karen. Large Scale GAN Training for High Fidelity Natural Image Synthesis. *International Conference on Learning Representations*, 2018.
- [77] Zhang, Richard and Isola, Phillip and Efros, Alexei A and Shechtman, Eli and Wang, Oliver. The unreasonable effectiveness of deep features as a perceptual metric. *Proceedings of the IEEE conference on computer vision and pattern recognition*, pages 586–595, 2018.
- [78] Kendall, Maurice G. A new measure of rank correlation. *Biometrika*, pages 81–93, 1938.
- [79] Kingma, Diederik P and Ba, Jimmy. Adam: A method for stochastic optimization. *arXiv preprint arXiv:1412.6980*, 2014.
- [80] Liu, Yilin and Li, Jiang and Pang, Yunkui and Nie, Dong and Yap, Pew-Thian. The devil is in the upsampling: Architectural decisions made simpler for denoising with deep image prior. *Proceedings of the IEEE/CVF International Conference on Computer Vision*, 12408–12417, 2023.
- [81] Cheng, Zezhou and Gadelha, Matheus and Maji, Subhansu and Sheldon, Daniel. A bayesian perspective on the deep image prior. *Proceedings of the IEEE/CVF Conference on Computer Vision and Pattern Recognition*, 5443–5451, 2019.

Appendix A Pseudocode of GI-NAS

We first elaborate on the pseudocode of GI-NAS in Algorithm 1. In the first loop, we select the optimal model G_{opt} by comparing the initial gradient matching loss among all the candidates. In the second loop, we optimize the parameters of the selected model G_{opt} to reconstruct the original data.

Algorithm 1 Gradient Inversion via Neural Architecture Search

Input: n : the size of the model search space; s : the random seed used to generate the model search space; \mathbf{g} : the uploaded real gradients; m : the maximum iteration steps for the final optimization;
Output: $\hat{\mathbf{x}}^*$: the generated images;

- 1: Build up the model search space according to n and s : $\mathcal{M} = \{G_1, G_2, \dots, G_n\}$ with the parameters $\Phi = \{\phi_1, \phi_2, \dots, \phi_n\}$
- 2: $\mathbf{z}_0 \leftarrow \mathcal{N}(0, 1)$, $loss_{min} \leftarrow +\infty$
- 3: **for** $i \leftarrow 1$ to n **do**
- 4: $loss_i \leftarrow \mathcal{D}(\mathcal{T}(F(G_i(\mathbf{z}_0; \phi_i))), \mathbf{g})$ // calculate the initial gradient matching loss
- 5: **if** $loss_i < loss_{min}$ **then**
- 6: $loss_{min} \leftarrow loss_i$, $G_{opt} \leftarrow G_i$, $\gamma_1 \leftarrow \phi_i$ // update the selection of G_{opt}
- 7: **end if**
- 8: **end for**
- 9: **for** $k \leftarrow 1$ to m **do**
- 10: $\gamma_{k+1} \leftarrow \gamma_k - \eta \nabla_{\gamma_k} \mathcal{D}(\mathcal{T}(F(G_{opt}(\mathbf{z}_0; \gamma_k))), \mathbf{g})$
- 11: **end for**
- 12: $\gamma^* \leftarrow \gamma_{m+1}$
- 13: **return** $\hat{\mathbf{x}}^* = G_{opt}(\mathbf{z}_0; \gamma^*)$

Appendix B More Experimental Results

B.1 Attacks at Larger Batch Sizes on CIFAR-10

We present the attack results at larger batch sizes on CIFAR-10 in Table 5. We conclude that GI-NAS outperforms all the compared methods with significant performance gains. For instance, GI-NAS achieves an improvement of 9.17 dB in terms of PSNR compared to GION at $B = 48$. GI-NAS still exhibits great superiority over existing gradient inversion methods when facing larger batch sizes.

Table 5: Quantitative comparison of GI-NAS to state-of-the-art gradient inversion methods on CIFAR-10 (32×32) with larger batch sizes when $B > 4$.

Metric	Batch Size	IG	GI	GGL	GIAS	GION	GI-NAS	Batch Size	IG	GI	GGL	GIAS	GION	GI-NAS
PSNR \uparrow SSIM \uparrow FSIM \uparrow LPIPS \downarrow	16	10.2647	11.2593	9.9964	11.1952	24.8746	30.5315	48	9.5446	10.2000	9.1200	9.6376	29.5312	38.7054
		0.2185	0.2431	0.1658	0.2638	0.9816	0.9948		0.1574	0.1697	0.1552	0.1652	0.9932	0.9983
		0.5254	0.5350	0.4988	0.5569	0.9869	0.9965		0.5112	0.5167	0.4869	0.5126	0.9949	0.9987
		0.6254	0.6225	0.6655	0.5804	0.0177	0.0035		0.6660	0.6571	0.7213	0.6554	0.0072	0.0020
PSNR \uparrow SSIM \uparrow FSIM \uparrow LPIPS \downarrow	32	9.5802	10.5863	9.4104	9.8669	28.6832	33.0586	96	9.2363	9.9500	8.8575	9.2982	28.9723	31.8026
		0.1595	0.2020	0.1481	0.1724	0.9892	0.9974		0.1402	0.1643	0.1516	0.2180	0.9878	0.9941
		0.5186	0.5325	0.4995	0.5180	0.9882	0.9984		0.4961	0.5238	0.4801	0.5365	0.9865	0.9941
		0.6598	0.6626	0.6922	0.6362	0.0218	0.0017		0.6865	0.6593	0.7248	0.7297	0.0227	0.0071

B.2 Attacks under Defense Strategies on CIFAR-10

We also report the attack results under various defense strategies on CIFAR-10 in Table 6. We apply the estimated gradient transformation $\mathcal{T}(\cdot)$ described in (6) to all the attacks and utilize the same defense strategies as in the earlier section of this paper: (1) *Gaussian Noise* [31] with a standard deviation of 0.1; (2) *Gradient Clipping* [31] with a clipping bound of 4; (3) *Gradient Sparsification* [33] with a pruning rate of 90%; (4) *Representative Perturbation (Soteria)* [35] with a pruning rate of 80%. We observe that GI-NAS again surpasses all the compared methods in almost all the circumstances with significant performance gains. For instance, GI-NAS achieves a PSNR increase of 9.52 dB than GION when the defense strategy is Gradient Sparsification [33]. The only exception is that GGL achieves better SSIM and LPIPS performance than GI-NAS when the defense strategy is

Table 6: Quantitative comparison of GI-NAS to state-of-the-art gradient inversion methods on CIFAR-10 (32×32) under various defense strategies with the default batch size $B = 4$.

Metric	Defense	IG	GI	GGL	GIAS	GION	GI-NAS	Defense	IG	GI	GGL	GIAS	GION	GI-NAS
PSNR \uparrow		8.8332	8.2797	10.3947	9.8146	9.7658	10.5192		9.6183	10.9486	10.4323	12.1328	30.3518	39.8739
SSIM \uparrow	Gaussian	0.1177	0.0976	0.1856	0.1301	0.0280	0.0375	Gradient	0.1592	0.2168	0.1862	0.3227	0.9920	0.9987
FSIM \uparrow	Noise	0.4844	0.4806	0.5123	0.4843	0.5945	0.6300		Sparsification	0.5151	0.5329	0.5223	0.6015	0.9951
LPIPS \downarrow		0.7258	0.7077	0.6255	0.7129	0.6752	0.6740		0.6895	0.6855	0.6298	0.5582	0.0047	0.0014
PSNR \uparrow		16.6203	11.5888	10.1373	17.9859	32.4744	36.2490		9.4103	10.2939	10.4217	15.5825	31.1003	34.1804
SSIM \uparrow	Gradient	0.5952	0.2851	0.1760	0.6703	0.9933	0.9985	Soteria	0.1404	0.1707	0.1889	0.5405	0.9900	0.9973
FSIM \uparrow	Clipping	0.7464	0.4976	0.5070	0.7751	0.9966	0.9992		0.5086	0.5086	0.5144	0.7133	0.9952	0.9986
LPIPS \downarrow		0.3811	0.6413	0.6205	0.3054	0.0029	0.0008		0.7008	0.6940	0.6335	0.3748	0.0038	0.0014

Gaussian Noise [31]. This can be attributed to the fact that the gaussian noise have severely damaged the gradients and the information carried inside the gradients is no longer suitable for gradient inversion. However, GGL can still generate natural images that possess some semantic features by the pre-trained GAN and obtain not bad performance even though the generated images are quite different from the original ones. This is also consistent with the defense auditing results on ImageNet that have been presented in previous part of this paper.

B.3 More Qualitative Results

We provide more qualitative results in Figure 7 and Figure 8. We observe that our reconstructed images are the closest to the original images, with less blemishes or stains than the results of GION. This proves that our adaptive network architecture search indeed helps the attackers obtain better implicit architectural priors and thus better remove the local noises.

B.4 Attacks on More FL Global Models

We show the performance of different methods when attacking more FL global models (e.g., LeNet-Zhu [11], ResNet-50 [74]) in Table 7. We note that GI-NAS realizes the best reconstruction results in all the tested cases. These results further demonstrate the reliability and generalizability of GI-NAS.

Table 7: PSNR results of GI-NAS and state-of-the-art gradient inversion methods when attacking various FL global models on CIFAR-10 (32×32) and ImageNet (256×256) with the default batch size $B = 4$.

Method	CIFAR-10			ImageNet		
	LeNet-Zhu	ResNet-50	ConvNet-32	LeNet-Zhu	ResNet-50	ConvNet-32
IG	11.9297	10.9667	12.3516	7.7175	10.9113	10.9081
GI	9.8537	10.8969	12.3560	6.9530	10.8914	10.8886
GGL	12.0546	9.3792	9.3348	11.8195	9.5354	10.4048
GIAS	24.7742	7.7656	8.0951	16.5229	11.0040	8.6696
GION	27.8141	28.3125	11.9893	19.2478	9.2080	23.9602
GI-NAS	30.1388	40.3566	13.3505	21.1847	11.2320	25.7824

We also find that the attack results on different FL global models are distinctively dissimilar even when applying the same gradient inversion method. This implies that future study may have a deeper look into the correlations between the gradient inversion robustness and the architecture of FL global model, and thus design more securing defense strategies from the aspect of network architecture.

Appendix C More Implementation Details

The learning rate η in (7) is set as 1×10^{-3} . We utilize the signed gradient descent and adopt Adam optimizer [79] when updating the parameters of G_{opt} . We choose the negative cosine similarity function as the distance metric $\mathcal{D}(\cdot, \cdot)$ when calculating the gradient matching loss $\mathcal{L}_{grad}(\cdot)$ in (6). We conduct all the experiments on NVIDIA GeForce RTX 3090 GPUs for small batch sizes and on A100 GPUs for large batch sizes.

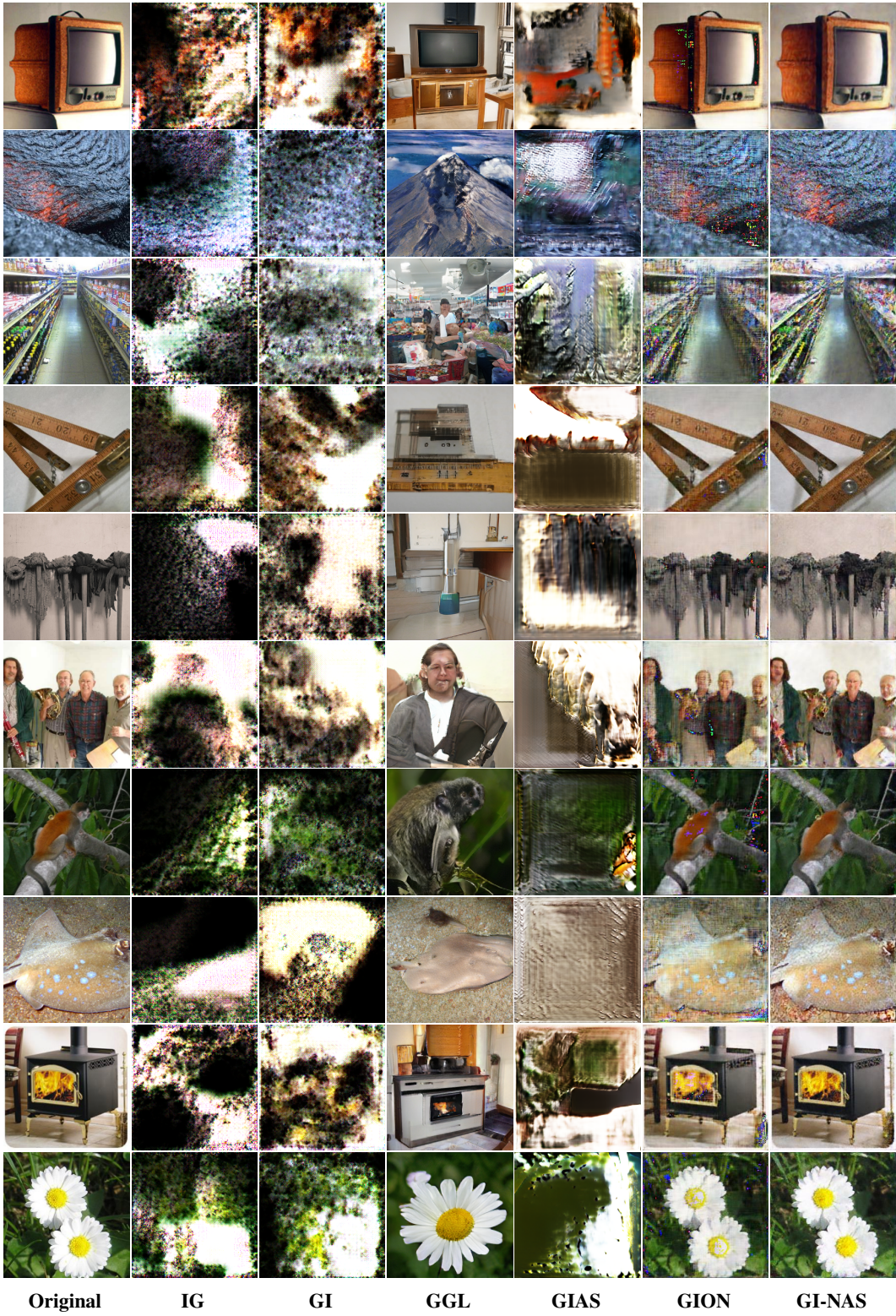
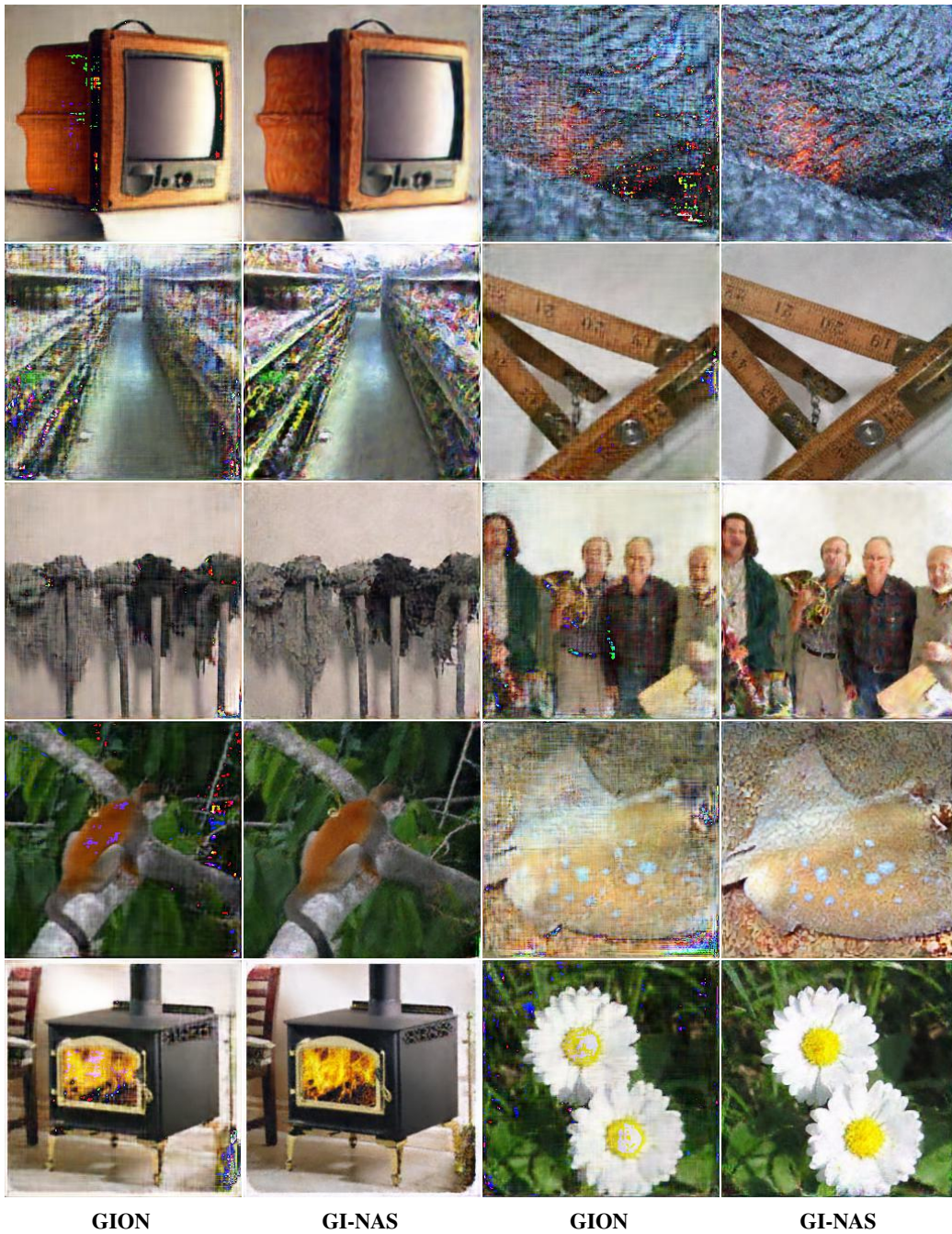


Figure 7: More qualitative results of different methods on ImageNet (256×256) with the default batch size $B = 4$.



GION

GI-NAS

GION

GI-NAS

Figure 8: More detailed qualitative comparisons between GION and GI-NAS on ImageNet (256×256) with the default batch size $B = 4$. Although GION also generates images that relatively resemble the original ones, we still easily observe many speckles or smudges when comparing it with GI-NAS.

Appendix D Limitations and Future Directions

In this paper, GI-NAS utilizes the initial gradient matching loss as the training-free search metric, which is intuitive but effective. Although we have empirically demonstrated that the initial loss is highly related to the final performance in Figure 6, it is still of great significance to further prove the effectiveness of this search metric with rigorous theoretical analysis. In the future work, we hope to provide more insightful theoretical results with regard to this search metric from various perspectives, such as the frequency spectrum [80, 73] or the implicit neural architectural priors [21, 81].

Appendix E Societal Impacts

We hope that the remarkable attack performance improvements of GI-NAS over existing methods may help raise the public awareness of such privacy threats, as the sensitive data would be more likely to be revealed or even abused. Moreover, we hope that the idea of this paper may shed new light on the gradient inversion community and facilitate the research in this field.